



Utilizing the drill cutting lip to extract Johnson Cook flow stress parameters for Al6061-T6

Charbel Y. Seif^a, Ilige S. Hage^b, Ramsey F. Hamade^{a,*}

^aMechanical Engineering Department, American University of Beirut, P.O. Box 11-0236, Riad El-Solh, Beirut 1107 2020, Lebanon

^bMechanical Engineering Department, Notre Dame University-Louaize, P.O. Box 72, ZOOUK, Zouk Mosbeh, Lebanon



ARTICLE INFO

Article history:
Available online 13 August 2019

Keywords:
Drilling
Forces
Constitutive equation
Johnson Cook
Oxley shear zone
Flow stress
Al-6061-T6

ABSTRACT

Owing to the chisel drill lip's complex geometric configuration, the material being cut witnesses great variations in strain, strain rate, and temperature along the cutting edge. This characteristic is explored in this work so that the drill point utilized as a material characterization tool to extract the flow stress parameters of the material cut. Specifically, the methodology, dubbed the Drill Lip Cutting Force Prediction Methodology (DLCFPM), utilizes a small number of pre-cored drilling experiments to extract the Johnson–Cook (JC) parameters for Aluminum Al6061-T6. Few drilling experiments are run to cover a wide range of drilling conditions: spindle speeds ranging from 1592 rpm rotational speed to 9868 rpm and drilling feed rates ranging from 0.08 mm/rev to 0.64 mm/rev.

For calculating the cutting forces numerically, DLCFPM employs a combination of (1) Oxley's predictive machining theory (extended thick shear zone analysis) and (2) analytical formulation for lip force generation. A custom optimization code is developed for numerically converging on an optimum set of JC parameters by matching simulated drilling torque values at the lip with those measured experimentally. For further corroboration, finite element (FEM) simulations are run using DLCFPM-found JC parameters. Numerically-simulated torque and thrust values are found to agree with those generated from the drilling experiments and with FEM results giving validity to the developed methodology for determining the JC parameters of Al6061-T6 from few drilling tests.

© 2019 CIRP.

Introduction and background

Constitutive equations have long been employed to simulate the mechanical response of solids under variable loading conditions of strain, ϵ , strain rate, $\dot{\epsilon}$, and temperature, T . To determine the parameters for such equations, experiments employing mechanical tests (e.g., tension, compression, or torsion) need to be conducted. Considering the great efforts typically involved in generating such material models, cutting experiments may be employed as an alternative method for determining such parameters. Cutting operations are characterized [1] by wide ranges of operating state variables of strain (1–10), strain rate (10^3 – 10^6 s⁻¹). This wide range of state variables gives rise to an opportunity to utilize cutting experiments as characterization techniques to extract material parameters of the workpiece being cut (e.g., [2]).

Starting from a limited number of drilling experiments, this work provides a methodology that identifies Johnson–Cook (JC)

constitutive model parameters. The workpiece material adopted is Aluminum 6061-T6 considering its widespread use in industry. Hamade and Ismail [3] studied aggressive drilling in aluminum and reported on applicable material flow stress models. However, given how widely accepted is JC formulation [4], this work is concerned with this type of material flow stress model typically reported as

$$\sigma = (A + B\epsilon^n) \left[1 + C \ln \left(\frac{\dot{\epsilon}}{\dot{\epsilon}_0} \right) \right] \left[1 - \left(\frac{T - T_r}{T_m - T_r} \right)^m \right] \quad (1)$$

where σ is the equivalent stress, the first two terms are the strain and strain rate hardening terms, respectively, and the third term accounts for temperature softening. Reported by [5] Eq. (1), ϵ is the equivalent strain, $\dot{\epsilon}/\dot{\epsilon}_0$ is the normalized strain rate defined as the ratio of the equivalent strain rate $\dot{\epsilon}$ to reference strain rate $\dot{\epsilon}_0 = 1$ s⁻¹, and $\left[1 - \frac{T - T_r}{T_m - T_r} \right]$ represents the material homologous temperature where T is operating material temperature, T_r is operating room temperature, and T_m is material melting temperature. A , B , C , n , m are five material parameters defined as Johnson cook yield strength, strength coefficient, strain rate constant, strain hardening exponent and temperature exponent respectively typically determined from fitting to experimental data.

* Corresponding author.
E-mail address: rh13@aub.edu.lb (R.F. Hamade).

Based on the application and the studied loading parameter ranges, different researchers utilized different experimental methods to determine the desired JC parameters. Table 1 lists a number of works that report the values of such parameters for Aluminum 6061-T6 including compression testing [5], Taylor impact test [6], dynamic punch tests [7], bullet-impact test [8], combined compression and orthogonal cutting tests [9], and orthogonal cutting tests [10]. Also based on orthogonal tests conducted on aluminum 6061-T6, Daoud et al. [11] reported updated JC parameters based on response surface methodology optimization combined with Oxley's [12] machining models using detailed work by Johnson et al. [5] as initial JC parameters. While values vary depending on the method, Johnson et al. [5] reported flow stress parameters for Aluminum 6061-T6 as 324 MPa, 114 MPa, 0.002, 0.42, 1.34 for A, B, C, n, and m, respectively. These parameters are applicable for strains up to 500%, strain rates up to 10^3 s^{-1} , and temperatures similar to those encountered in machining operations. For all cases listed, the 6061-T6 material melting temperature identified as 582 °C.

Oxley [13] developed a predictive machining theory based on parallel-sided thick shear zone analysis that accounts for strain, strain rate, and temperature-dependent material flow stress. Utilizing Oxley's thick shear zone approach, this work employs a drill lip model for calculating generated cutting forces based on drilling conditions and JC material model. Using an optimization scheme, JC material model parameters are determined by minimizing the error between calculated drill bit cutting lip forces and experimentally measured machining forces at matching cutting conditions of rotational speed and feed rate. This work also utilizes FEM simulations for further corroboration of the accuracy of the obtained JC flow stress parameters. Employing the drill's complex cutting lip geometry allows us to benefit from the significant variations in cutting parameters and the resulting material state variables encountered along the lip cutting edge. Unlike a large number of orthogonal machining tests typically required (e.g., [9–11]), only a small number of drilling tests would be needed for determining material constitutive equation parameters.

The flowchart in Fig. 1 summarizes the DLCPFM methodology. The methodology incorporates as inputs the drill geometric attributes (nominal drill diameter, D (mm)), web thickness to diameter ratio, $2w/D$, point angle, $2p$ (degrees), nominal helix angle, β_0 (degrees), chisel edge angle, ψ (degrees) and cutting conditions (rotational speed (RPM), feed (f : mm/rev)).

Section "Two-dimensional orthogonal cutting shear zone model" summarizes shear zone formulations based on the thick shear zone analysis. Section "Extending shear zone formulation for JC-type constitutive equation" reports on the extension of the thick shear zone model by incorporating a JC type material flow stress model Lalwani et al. [14] and validates the extended analysis against literature-reported results. Developed in Section "Oblique cutting model (based on Lin) [15]" is a three-dimensional (3D) cutting force prediction model using oblique cutting force

transformations based on [15] coupled with thick shear zone analysis [13]. Section "Extended JC shear zone approach applied to drillcutting lip force prediction" couples the 3D oblique transformation module with extended Oxley's thick shear zone cutting prediction module [16]. The desired JC parameters determined in Section "Determining the Johnson–Cook equation parameters for Al 6061-T6" by minimizing differences between predicted torque values generated by the methodology and the experimental drilling torque measurements. Section "Validation of methodology using FEM simulations" reports on FEM simulations of the drill's lip forces using the newly found JC parameters. Section "Comparison of predicted drilling forces versus FEM and experimental measurements" compares history profiles of torque and thrust forces covering a wide range of drilling parameters of speed and feed as calculated from DLCPFM using JC parameters found in Ref. [5] and those found in Section "Validation of methodology using FEM simulations", FEM model section, and experimentally collected torque and thrust data (Section "Comparison of predicted drilling forces versus FEM and experimental measurements").

Drilling experiments

Drilling tests were conducted using pre-cored holes of diameters larger than the chisel. A 10 mm diameter HSS classical chisel drill was utilized with the cutting point's geometric attributes as listed in Table 2.

Cutting forces were collected using four-channel (F_x , F_y , F_z , and torque) Kistler rotary dynamometer (model 9124B) mounted on a Deckel Maho machining center model DMU 80P CNC milling unit having 12,000 rpm maximum spindle speed and 130Nm maximum torque. Applied median filter for noise dampening in collected thrust force and torque measured data. The dynamometer has an uncertainty of $\pm 4 \text{ N}$ and $\pm 0.3 \text{ Nm}$ for measured forces and torque, respectively. Dry (no coolant) experiments were conducted using fresh tools. Cylindrical workpieces with a diameter of 20 mm were utilized with pre-cored holes of 2.5 mm, 3.5 mm, 5.5 mm, and 7.5 mm diameters. A photograph of the dynamometer mounted in the machine tool shown in Fig. 2(a) and two photographs with pre-cored 3.5 mm diameter hole and drilled workpiece shown in Figs. 2(b) and (c), respectively.

Generated torque and thrust force data were collected as the cutting lip engaged with workpiece after applying 20 data point median filter. The profiles plotted in Fig. 2(d) correspond to 2.5 mm pilot hole diameter, spindle speed of 9868 rpm, and 0.64 mm/rev feed rate. Drilling torque and thrust measurements are collected for all cases listed in Table 3. All experiments were conducted using fresh tools to eliminate tool wear contribution to forces.

Shear zone formulations for the cutting lip force prediction

Discussed in this section are the analytical formulations employed where numerically are calculate cutting forces along the lip.

Table 1
Reported JC-type material flow stress parameters for Aluminum 6061-T6 material.

Reference	A (MPa)	B (MPa)	n	C	m	$\epsilon_0 (\text{s}^{-1})$	Test conducted
[4]	324	114	0.42	0.002	1.34	1	Compression tests
[5]	164	211	0.465	0.00197	1.419	1	Taylor compression tests
[6]	335	85	0.11	0.012	1	1	Punch tests
[7]	270	138.2	0.1792	0.1301	1.34	597.2	Bullet test
[8]	275	86	0.39	0.05810-194.091 t_c -0.00306V	1	0.01	Orthogonal machining/compression tests
[10]	250	79.7	0.499	0.0249	1.499	1	Orthogonal machining
[9]	337	136	0.0025	0.5	1.34	1	Orthogonal machining

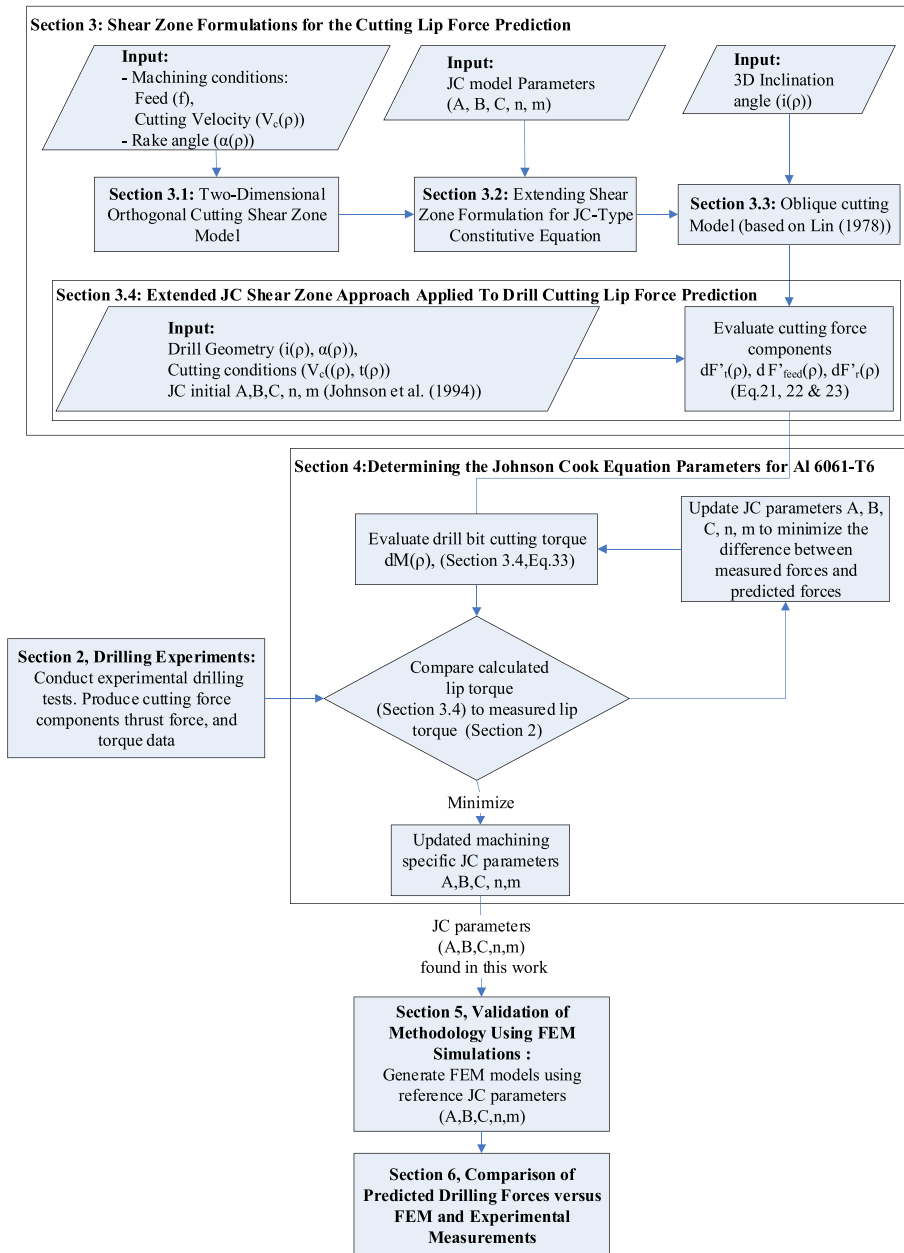


Fig. 1. Extracting JC parameters based on the proposed DLCPM methodology from drilling tests.

Table 2
Classical chisel drill attributes.

HSS drill Parameters	Values
Nominal diameter, D (mm)	10
Web thickness to diameter ratio, 2w/D	0.15
Point angle, 2p (degrees)	119
Nominal helix angle, β_0 (degrees)	17
Chisel edge angle, ψ (degrees)	125

Two-dimensional orthogonal cutting shear zone model

Oxley [12] analytical cutting model is based on a primary shear deformation zone (thickness S_1) and secondary tool-chip interface deformation zone (thickness S_2).

Fig. 3 is a diagram that illustrates orthogonal cutting's salient features including the cutting wedge with a rake face angle (α) as it removes an uncut chip thickness (t_1). By shearing along a shear plane (AB) that makes an angle (ϕ) with the horizontal, the cut material is transformed into a chip of thickness (t_2). Also shown in Fig. 3 are the resultant cutting force (R_F), cutting tool normal force (N), cutting tool friction force (P), shear plane force (F_s), normal to shear plane force (F_n), feed (F_{feed}), and tangential (F_t) force components.

The analysis evaluates the shear stress distribution along the primary deformation zone centered at the shear plane (AB) to find the balancing, normal stress (estimated along the secondary deformation zone at the tool/chip interface) by varying the shear angle (ϕ), primary deformation zone thickness ratio (C'), and secondary deformation zone thickness ratio (δ). The parameter

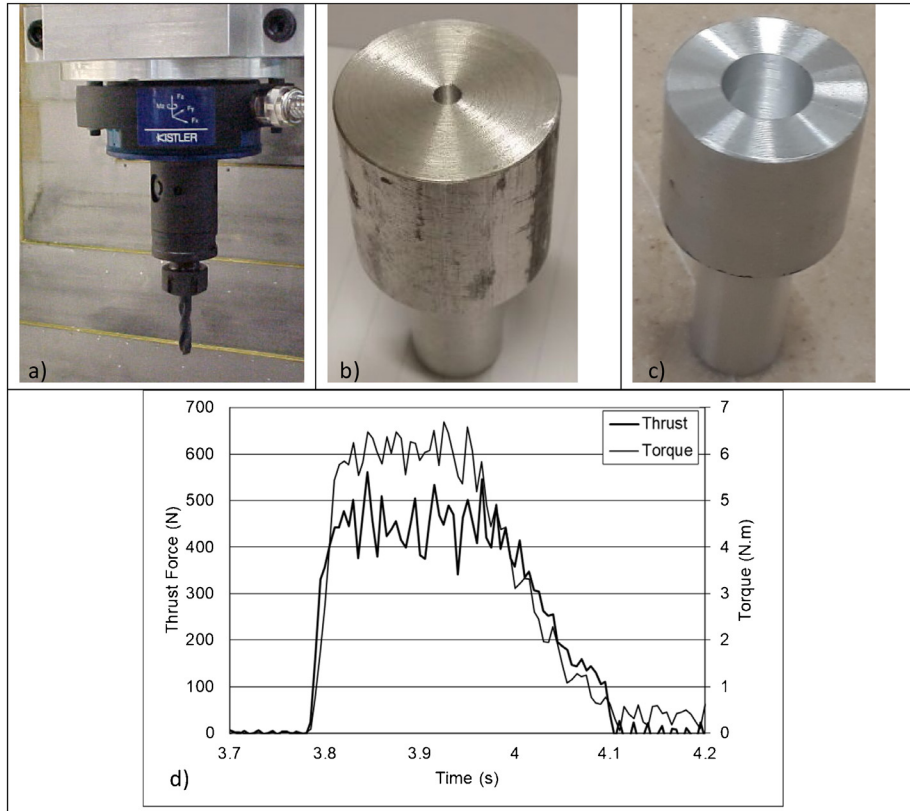


Fig. 2. Photographs of (a) drilling set up, (b) Al 6061-T6 workpiece with a pre-cored hole (diameter = 3.5 mm), (c) fully drilled workpiece, and (d) generated torque and thrust force profiles.

Table 3
Drilling tests at the drilling process parameters listed.

Experiment number	Pre-cored hole diameter (mm)	Feed (mm/rev)	Spindle rotation (RPM)
1	2.5	0.64	9868
2	3.5		
3	5.5		
4	7.5		
5	3.5	0.32	6838
6	5.5	0.16	3183
7	7.5	0.08	1592

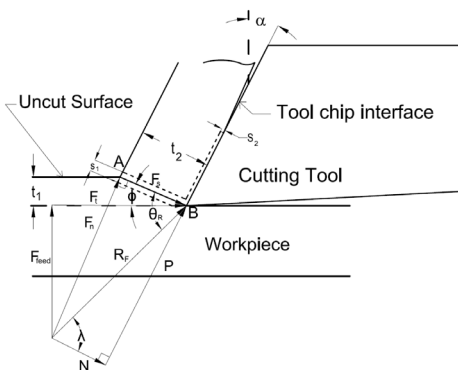


Fig. 3. Parameters and force components in orthogonal cutting.

$C' = l/S_1$, defined as the ratio of the length (l) of the shear plane AB to the thickness of the primary shear zone (S_1). The parameter $\delta = S_2/t_2$, estimated as the ratio of the thickness of the secondary deformation zone located at the tool-chip interface (S_2) to the cut chip thickness, t_2 , defined in Eq. (2) where

$$t_2 = \frac{t_1 \cos(\phi - \alpha)}{\sin(\phi)} \quad (2)$$

Fig. 4 is a flowchart that illustrates the shear zone solution and how δ , C' , and ϕ are varied [12] for each iteration. For each condition of cutting speed, V , and feed, f , the values of parameters δ , C' , ϕ are varied between 0.005 and 0.2, 2 and 10, and 5 and 45°, respectively.

The analysis is performed at all combinations of δ , C' , and ϕ . Solutions for material flow stress parameters are found for the case that satisfies the balance of forces between the primary deformation and secondary deformation zones. The angle between the resultant force, R_F , and shear plane direction is θ_R calculated based on Eq. (3) as

$$\tan(\theta_R) = 1 + 2\left(\frac{\pi}{4} - \phi\right) - C' n' \quad (3)$$

where n' is the material specific strain hardening exponent found from the material power equation $\sigma = \sigma_1 \epsilon^{n'}$ [12] and is a function of the shear zone average temperature, T_{AB} , and shear zone deformation speed, V_s . Using Eq. (4), for each value of the calculated resultant angle, θ_R , a corresponding friction angle λ is estimated [17] as

$$\theta_R = \phi + \lambda - \alpha \quad (4)$$

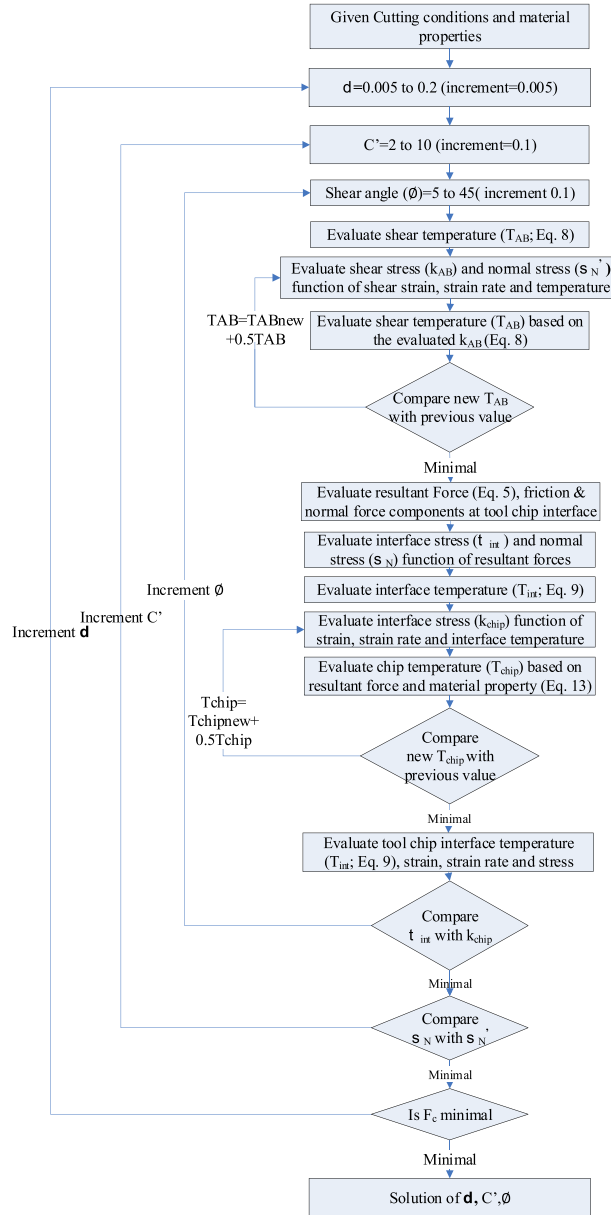


Fig. 4. Flow chart for the shear zone solution [11].

The resultant cutting force R_F is found from Ref. [12] reported in Eq. (5).

$$R_F = \frac{F_s}{\cos(\theta_R)} = \frac{k_{AB} t_1 W}{\sin(\phi) \cos(\theta_R)} \quad (5)$$

Using the constitutive model of the work material, average shear stress, k_{AB} , occurring at the shear plane (AB) is estimated as a function of mean strain, γ_{AB} , strain rate, $\dot{\gamma}_{AB}$, and temperature, T_{AB} , of the shear zone. Eq. 6, calculate the average shear strain, γ_{AB} , is a function of cutting tool rake angle, α , and shear angle, ϕ , as

$$\gamma_{AB} = \frac{\cos(\alpha)}{2 \sin(\phi) \cos(\phi - \alpha)} \quad (6)$$

Average strain rate, $\dot{\gamma}_{AB}$, at the parallel-sided thick shear zone is a function of the primary deformation zone thickness ratio, C' , shear plane deformation speed, V_s , and shear plane length, l , using

Eq. (7) as

$$\dot{\gamma}_{AB} = \frac{C' V_s}{l} \quad (7)$$

Average machining temperatures along the primary shear zone, T_{AB} , and secondary (tool-chip interface) region, T_{int} , are evaluated utilizing Eqs. (8) and (9), proposed by Ref. [18]

$$T_{AB} = T_w + \eta \frac{(1 - \beta_T) F_s \cos \alpha}{\rho_d C_p t_1 W \cos(\phi - \alpha)} \quad (8)$$

$$T_{int} = T_w + \frac{(1 - \beta_T) F_s \cos \alpha}{\rho_d C_p t_1 W \cos(\phi - \alpha)} + \psi \Delta T_m \quad (9)$$

where T_w is the initial work temperature, $\eta=0.7$ is a factor accounting for plastic deformation occurring outside the shear

zone utilized by Ref. [12]. ΔT_m is the maximum temperature rise in the chip and the factor ψ with a value of 0.6 assigns T_{int} to an average value. The density and specific heat of the work material are ρ_d and C_p , respectively. The term β_T is the proportion of heat conducted into the work and is estimated using [18] empirically determined Eqs. (10) and (11)

$$\beta_T = 0.5 - 0.35 \log(R_T \tan \phi) \quad \text{for } 0.04 < R_T \tan \phi < 10 \quad (10)$$

$$\beta_T = 0.3 - 0.15 \log(R_T \tan \phi) \quad \text{for } R_T \tan \phi > 10 \quad (11)$$

With Eq. (12) defining R_T being a non-dimensional thermal number function of density, ρ_d , specific heat, C_p , cutting speed V , uncut chip thickness, t_1 , and workpiece thermal conductivity, K .

$$R_T = \frac{\rho_d C_p V t_1}{K} \quad (12)$$

The ratio of the average (ΔT_c) to maximum (ΔT_m) chip temperature rise is defined in Eq. (13) & (14) reported by Ref. [18] as

$$\log\left(\frac{\Delta T_m}{\Delta T_c}\right) = 0.06 - 0.195 \delta \left(\frac{R_T t_2}{h}\right)^{0.5} + 0.5 \log\left(\frac{R_T t_2}{h}\right) \quad (13)$$

where $\delta = S_2/t_2$ is the secondary deformation zone thickness ratio, t_2 is chip thickness, R_T is the non-dimensional thermal number Eq. (12), ΔT_c is the average chip temperature rise [19]

$$\Delta T_c = \frac{P \sin(\phi)}{(\rho C_p t_1 w \cos(\phi - \alpha))} \quad (14)$$

and h is the tool/chip contact length reported in Eq. (15)

$$h = \frac{t_1 \sin \theta}{\cos \lambda \sin \phi} \left[1 + \frac{C' n'}{3(1 + 2(\pi/4 - \phi) - C' n')} \right] \quad (15)$$

The force components F_c , F_r , P , N (Fig. 3) are determined [17] as a function of the resultant force, R_F , cutting rake angle, α , and friction angle, λ , at the δ , C' , and ϕ iteration as illustrated in Fig. 4. For each combination value for δ and C' , a solution for the shear angle, ϕ , is found for the corresponding shear angle that provides equilibrium between resultant forces transmitted through the shear plane and the chip-tool interface forces where $\tau_{int} = k_{chip}$ condition is satisfied. The shear stress generated by friction forces at the tool/chip interface, τ_{int} , is estimated based on dividing the cutting tool friction force (P) by the tool-chip contact area ($h w_c$) where h is the tool-chip contact length Eq. (15) and w_c is the chip width. The term k_{chip} is calculated using a material flow stress model of Eq. (16).

$$\sigma = \sigma_1 \varepsilon^{n'} \quad (16)$$

where operating material stress is estimated based on the chip's strain velocity-modified temperature occurring at the tool/chip interface secondary deformation zone. The terms σ_1 , ε , and n' are material effective stress, effective strain, and material specific temperature-modified strain hardening exponent, respectively.

For each δ value, Fig. 4 illustrates the solution of the primary deformation zone thickness ratio, C' , which is found when the condition $\sigma'_N = \sigma_N$ is satisfied. The term σ_N is the uniform normal stress at the chip-tool interface based on calculated cutting tool normal force, N , and the tool-chip contact area ($h w_c$).

The normal stress, σ'_N , is determined using Eq. (17) defining stress boundary at point B (Fig. 3) function of material stress at the shear plane, k_{AB} , rake angle, α , and the temperature modified strain hardening index n' as

$$\sigma'_N = k_{AB} (1 + 0.5\pi - 2\alpha - 2C' n') \quad (17)$$

Considering the plastic zone caused by friction work at the tool/chip interface and assuming that thickness S_2 of the secondary deformation zone is determined from minimum work principle, secondary deformation zone thickness ratio, δ , is obtained for the case where a combination of strain rate and temperature results yields minimum value of cutting force, F_c .

The combined solution for δ , C' , and ϕ is found for the case where solution values meet the following criteria simultaneously (as illustrated in Fig. 4)

- 1- Minimum F_{chip}
- 2- $\sigma'_N = \sigma_N$
- 3- $\tau_{int} = k_{chip}$

Oxley [12] validated the thick shear zone model by comparing his findings against orthogonal cutting experiments employing 0.2% and 0.38% carbon steels. To corroborate our findings, Oxley's results were replicated with a near perfect match as reported in the supplementary Tables S-1-a, and S-1-b.

Extending shear zone formulation for JC-Type constitutive equation

To utilize Oxley's thick shear zone analysis using material models, Lalwani et al. [14] conceived a methodology to replace the velocity-modified temperature term, Eq. (18)

$$T_{mod} = T[1 - 0.09 \log(\dot{\varepsilon})] \quad (18)$$

as initially advanced by Oxley [12] to account for combined strain rate and temperature effects on material properties. Utilizing low carbon steel, high order curve-fitting equation was used to describe the relation between T_{mod} and both uniaxial flow stress, σ_0 , at strain $\varepsilon = 1$ and the strain hardening index, n' , where shear stress expressed in Eq. (19) as

$$k = \frac{\sigma_0 \varepsilon^{n'}}{\sqrt{3}} \quad (19)$$

Lalwani et al. [14] extension of Oxley's thick shear zone to utilize flow stress model of the JC form follows the algorithm described by the flowchart in Fig. 4. The extension substitutes the modified temperature expression by introducing a strain-hardening exponent parameter defined in Eq. (20)

$$n_{eq} = \frac{n B \varepsilon_{AB}^n}{A + B \varepsilon_{AB}^n} \quad (20)$$

where A , B , and n are the JC parameters and ε_{AB} is the shear plane strain.

Having discarded strain-rate modified temperature, the analysis becomes capable of accommodating state variables as independent parameters. Solutions for δ , C' , and ϕ are then found using the convergence criteria described in Section "Two-dimensional orthogonal cutting shear zone model". For validation of the numerical code of this module, a comparison is made between the cutting forces calculated in this work by the extended shear zone approach utilizing JC formulation and results reported by Lalwani et al. [14] corresponding to the same cutting conditions and work material (0.38% carbon steel). Values generated in this work for the cutting force components in the velocity direction (F_t) and thrust force (F_{feed}) are found to be in good agreement with cutting force values reported by Lalwani et al. [12] as summarized in the supplementary Table S-2.

Oblique cutting model (based on Lin) [15]

To utilize the JC extended shear zone analysis in modeling three-dimensional drilling forces, an analytical transformation from 2D orthogonal forces to oblique 3D oblique forces is necessary. Lin [15] developed kinematical and geometrical

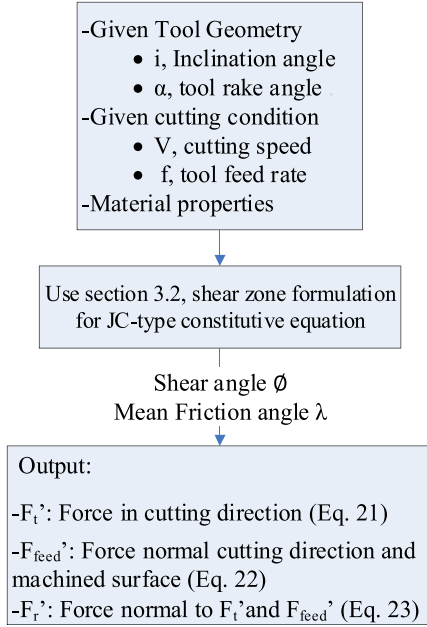


Fig. 5. Oblique cutting model based on the shear zone formulation [14].

transformations allowing for extending the thick shear zone orthogonal model application for oblique cutting. The flow chart in Fig. 5 illustrates the algorithm of this treatment.

The analysis considers the chip flow in the plane normal to the cutting edge as orthogonal (plain strain) flow. The oblique machining processes may then be divided into two simultaneous steps

- Orthogonal cutting in the tool normal plane.
- Chip sliding and shearing in a direction parallel to the cutting edge.

Cutting velocity (V) is shown in Fig. 6 to have been resolved into two components in terms of tool inclination angle, i , with $V = V \cos(i)$ and $V' = V \sin(i)$ being velocity components normal and parallel to the cutting edge, respectively. Force components F_t , F_{feed} , and P are the cutting force, thrust force, and friction force components in the tool normal plane, respectively, and are calculated based on extended shear zone formulation (Section “Extending shear zone formulation for JC-type constitutive equation”).

Considering geometrical relations, the oblique cutting, F_t' , thrust, F_{feed}' , and radial F_r' force components normal to F_t' and F_{feed}' are denoted in Fig. 6, and defined in Eqs. (21)–(23) as a function of force components in the tool normal plane F_t , F_{feed} , and P as

$$F_t' = F_t \cos(i) + P \tan(\eta_c) \sin(i) \quad (21)$$

$$F_{feed}' = F_{feed} \quad (22)$$

$$F_r' = F_t \sin(i) - P \tan(\eta_c) \cos(i) \quad (23)$$

The chip flow angle, η_c , is determined by Ref. [17] reported in Eq. (24) as a function of geometric features consisting of the rake angle, α , inclination angle, i , and cutting conditions dependent feature consisting of shear angle, ϕ , and mean friction angle along

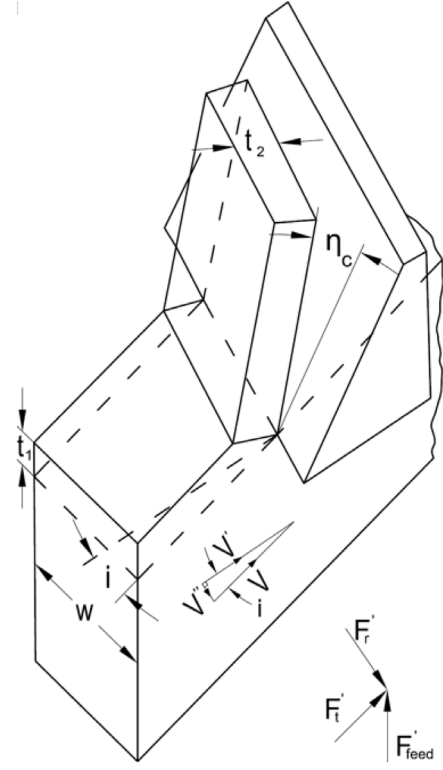


Fig. 6. Oblique cutting parameters and force components [14].

the tool-chip interface, λ , as

$$\tan(\eta_c) = \frac{\tan(i) \cos(\alpha)}{\tan(\phi + \lambda)} + \sin(\alpha) \tan(i) \quad (24)$$

Extended JC shear zone approach applied to drill cutting lip force prediction

Having adopted the orthogonal to oblique force transformation Lin [15], identifying the drill bit cutting lip varying oblique parameters becomes necessary for estimating cutting lip forces. Fig. 7(a, b) shows the salient features of the standard twist drill where the chisel edge is located at the drill's center with width, $2w$, and helical cutting lips having a point angle, $2p$, that meets the drill bit flute at helix angle, β_0 . For calculating cutting forces at the cutting lip, Williams [20] and Wiryacosol and Armarego [16] subdivided the cut material into a finite series of discrete elements (each representing an oblique cut) with the combined chip flow direction. Each element is associated with characteristic cutting speed, web angle, local helix angle, inclination angle, rake angle, and non-dimensional radial coordinate, ρ , defined in Eq. (25) as the ratio of drill lip elemental radius r divided by the drill bit radius, R , as

$$\rho = \frac{r}{R} \quad (25)$$

The cutting speed along the lip is a function of rotational speed, ω , and varies as a function of normal radius described in Eq. (26).

$$V(\rho) = \omega R \rho \quad (26)$$

Web angle, θ , (ρ) is related to w , R , and ρ as reported in Eq. (27)

$$\theta(\rho) = \sin^{-1} \left(\frac{w}{R \rho} \right) \quad (27)$$

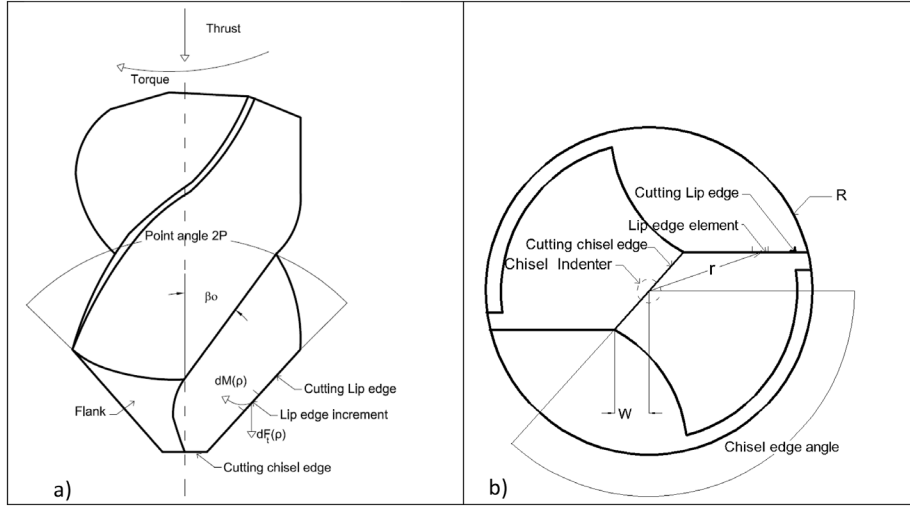


Fig. 7. Features and geometry of the cutting point of the traditional drill (a) front view, (b) top view.

Local helix angle, $\beta(\rho)$, is a function of nominal helix angle β_0 and ρ as stated in Eq. (28)

$$\beta(\rho) = \tan^{-1}(\rho \tan(\beta_0)) \quad (28)$$

The oblique cutting angle, $i(\rho)$, varies along the lip and defined as the angle formed between the cutting velocity vector and the normal to the cutting edge velocity vector, using Eq. (29) related to drill bit half point angle (p) and to $\theta(\rho)$.

$$i(\rho) = \sin^{-1}(\sin(p)\sin(\theta(\rho))) \quad (29)$$

Measured in a plane normal to the cutting edge, the effective rake angle, α_f , reported in Eq. (30) is defined as [21] the angle between the plane parallel to the drill axis containing the cutting edge and the plane tangent to the flute face at the cutting edge as

$$\alpha_f(\rho) = \tan^{-1}\left(\frac{\tan(\beta(\rho))\cos(\theta(\rho))}{\sin(p) - \tan(\beta(\rho))\cos(p)\sin(\theta(\rho))}\right) \quad (30)$$

Normal rake angle is described by Eq. (31)

$$\alpha_n(\rho) = \alpha_f(\rho) - \gamma_d(\rho) \quad (31)$$

where the angle $\gamma_d(\rho)$ defined in Eq. (32) results from projecting the velocity vector onto the normal plane and is determined from

$$\gamma_d(\rho) = \tan^{-1}(\tan(\theta(\rho))\cos(p)) \quad (32)$$

Fig. 8 illustrates the variations of the salient geometric angles as a function of non-dimensional radius along the drill bit cutting lip edge as predicted by Eqs. (27), (28), (29) and (31). Cutting action is more efficient at the lip margin where large positive rake angle and higher cutting velocities coincide contrary to the region adjacent to the chisel edge where concurrent negative rake angle and low cutting velocity reduces cutting efficiency. Taking advantage of the geometric tool variability along the drill lip, Hamade et al. [22] successfully extracted material specific cutting force parameters for Aluminum 6061-T6. The different geometric lip parameters are defined and are then combined with modified oblique cutting thick shear zone approach (Section “Oblique cutting model (based on Lin [14])”) based on Lalwani et al. [13] extended Oxley’s thick shear zone analysis (Section “Extending shear zone formulation for JC-type constitutive equation”).

Illustrated in Fig. 9 is the incremental force prediction flowchart according to Williams [20].

Where estimates of incremental torque (ρ), Eq. (33) and incremental thrust force (ρ) values become possible using Eq. (34) as a function of lip incremental edge oblique cutting force (F_t), oblique thrust force (F'_{feed}) and F'_R force components normal to F_t and F'_{feed} components as

$$dM(\rho) = \rho F'_t(\rho) \quad (33)$$

$$dF_t(\rho) = F'_{feed}(\rho)\sin(p) - F'_R(\rho)\cos(p) \quad (34)$$

Determining the Johnson–Cook equation parameters for Al 6061-T6

Having developed the verified drill cutting lip force prediction methodology (DLCPM) based on material model and drilling

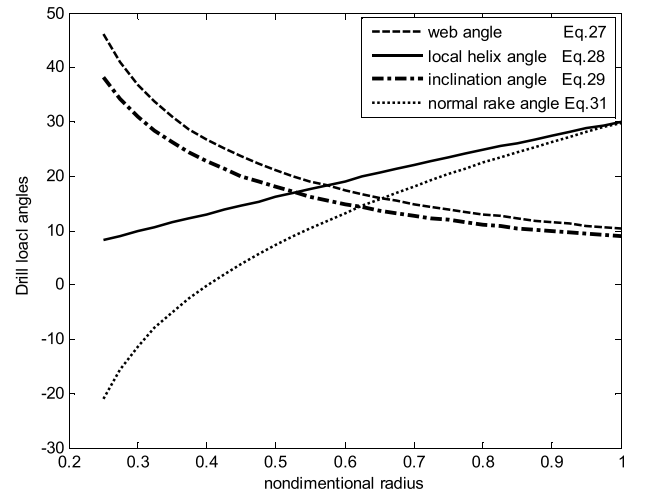


Fig. 8. Variations of the geometric angles along the cutting lip as a function of non-dimensional radius.

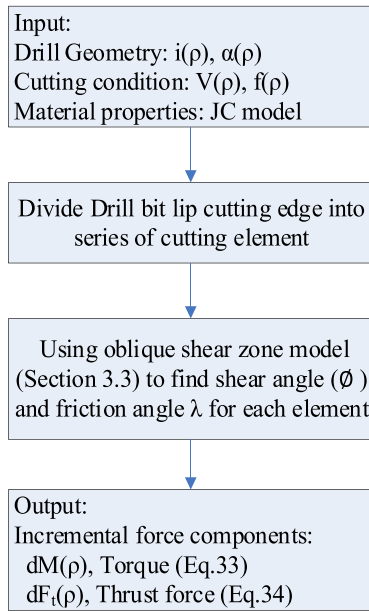


Fig. 9. Lip force prediction module [19].

conditions, JC material parameters determined by matching DLCFPM-determined lip torque values versus experimental torque values (Section “Determining the Johnson–Cook equation parameters for Al 6061-T6”). The DLCFPM methodology is implemented numerically as MATLAB® code that divides the lip into a series of cutting edges. Assigned to each segment are individual geometric attributes (Fig. 8) and cutting parameters (cutting speed and uncut

chip thickness). Considering drilling parameters (Table 1) and utilizing the extended JC shear zone module with JC parameters (Section “Oblique cutting model (based on Lin) [14]”), cutting forces were determined along the lip for 2.5 mm, 3.5 mm, 5.5 mm, and 7.5 mm pre-cored-holes. As the code runs and the lip progressively engages the workpiece, JC parameters are automatically adjusted (Fig. 1) to minimize the difference between calculated and measured torque values according to Eq. (35).

$$\min \left[\sqrt{\sum \left(M(\rho)_{measured} - M(\rho)_{predicted} \right)^2} \right] \quad (35)$$

Curve fitting is done using a custom MATLAB® code based on nonlinear least-squares optimization with the convergence criterion of 10^{-9} and maximum iteration number of 1000. For a defined search range, the optimization code identifies parameters that meet the global minimum criteria for the objective function Eq. (35) by establishing global and local quadratic convergence targets. The top rows in Table 4 list the lower and upper limits for the searching range for the JC parameters: A, B, C, n, and m. Listed in Table 4 are the results of four simulation cases (case #1 through #4) while DLCFPM searched for the optimum set of JC parameters. Case #1 is the control case where the values of the five parameters reported by Johnson et al. [5] for Aluminum 6061-T6 used as initial parameters. For cases #2, 3, and 4, randomly assigned initial sets of JC parameters were used. Utilizing Eq. (35) with the searching ranges subject to the convergence criteria, the DLCFPM optimization scheme converged to one set of parameter values for the five JC parameters A, B, C, n, and m of 317.54, 108.90, 0.0015, 0.43, and 1.29, respectively. These optimal JC parameter values resulted in numerical cutting forces profiles that duplicate the experimentally recorded data (Figs. 13,16).

Shown in Fig. 10 are conversion histories of the five (5) JC parameters, A, B, C, n, and m versus iteration number (case #1).

Table 4
JC parameters: ranges, initial assigned values, and determined values.

JC parameters		A	B	C	N	m
Searching range	Lower limit	290	90	0.0005	0.3	1.1
	Upper limit	350	140	0.004	0.6	1.4
Case #1	Initializing parameters from Johnson et al. [4]	324	114	0.002	0.42	1.34
	Found parameters	317.54	108.90	0.0015	0.43	1.29
Case #2	Random initial parameter values	350	100	0.001	0.4	1.2
	Found parameters	317.54	108.91	0.0015	0.43	1.29
Case #3	Random initial parameter values	270	130	0.005	0.2	1.2
	Found parameters	317.53	108.89	0.0015	0.43	1.29
Case #4	Random initial parameter values	100	400	1	0	2
	Found parameters	317.54	108.91	0.0015	0.43	1.29

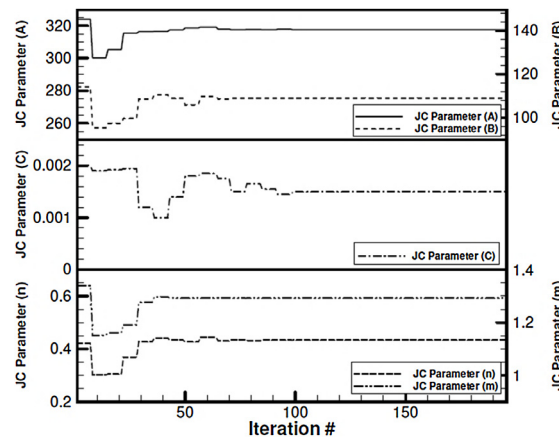


Fig. 10. Typical conversion histories of JC parameters A, B, C, n, and m versus iteration number.

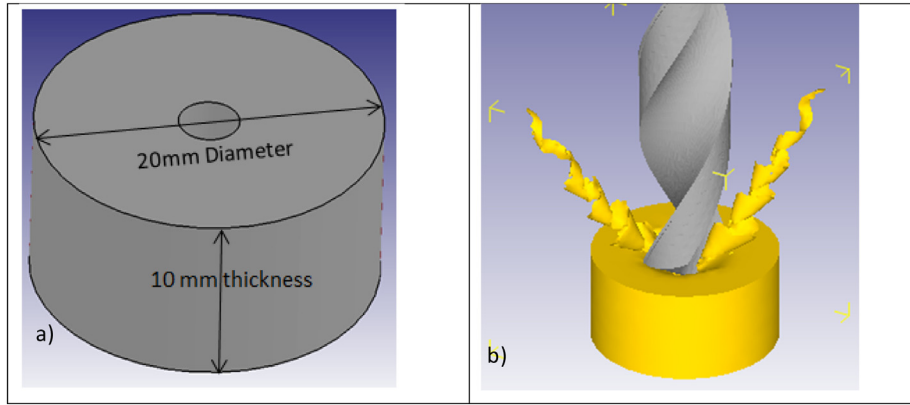


Fig. 11. Workpiece (a) showing the pre-cored pilot hole and (b) drilled in FEM (showing chip generation).

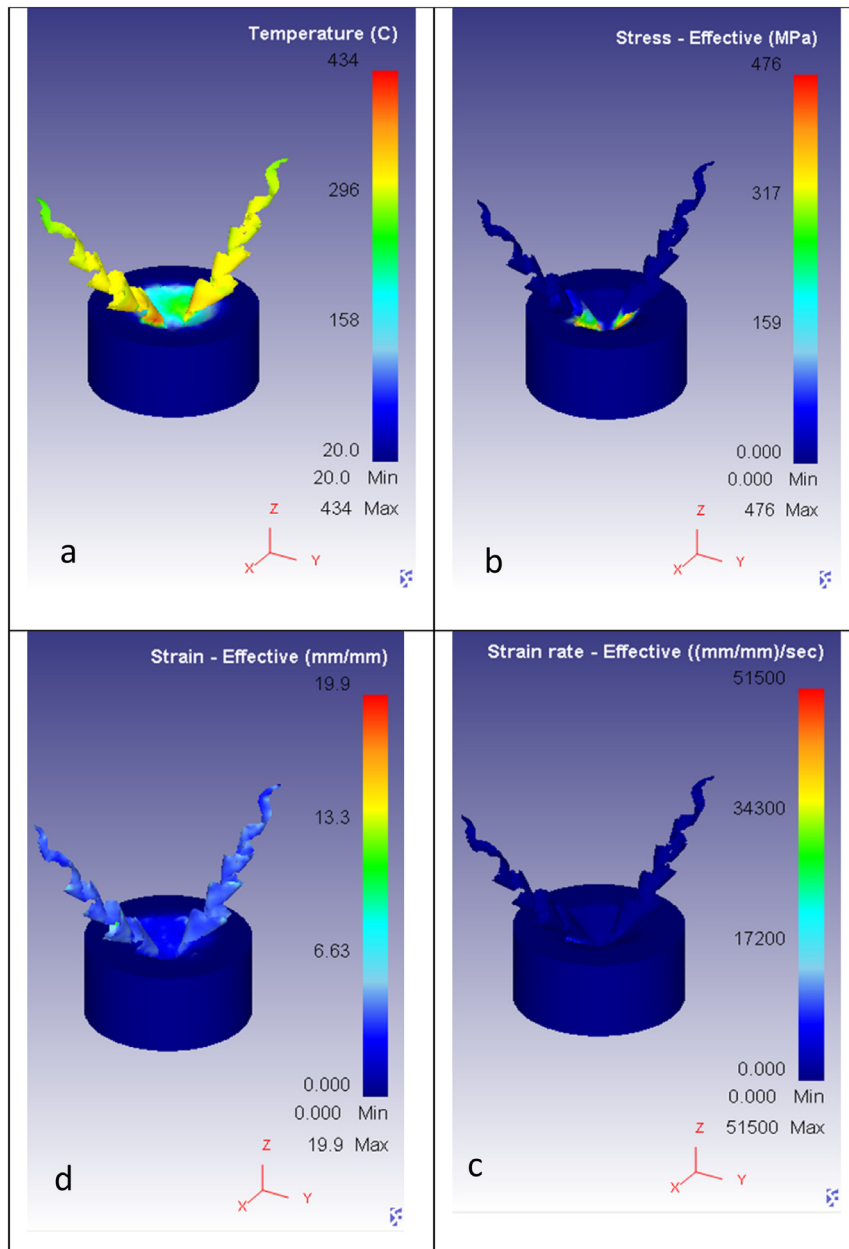


Fig. 12. FEM results for plots of (a) temperature, (b) effective stress, (c) strain, and (d) strain rate for the 2.5 mm pre-cored workpiece simulation (rotational speed of 9868 rpm and feed of 0.64 mm/revolution).

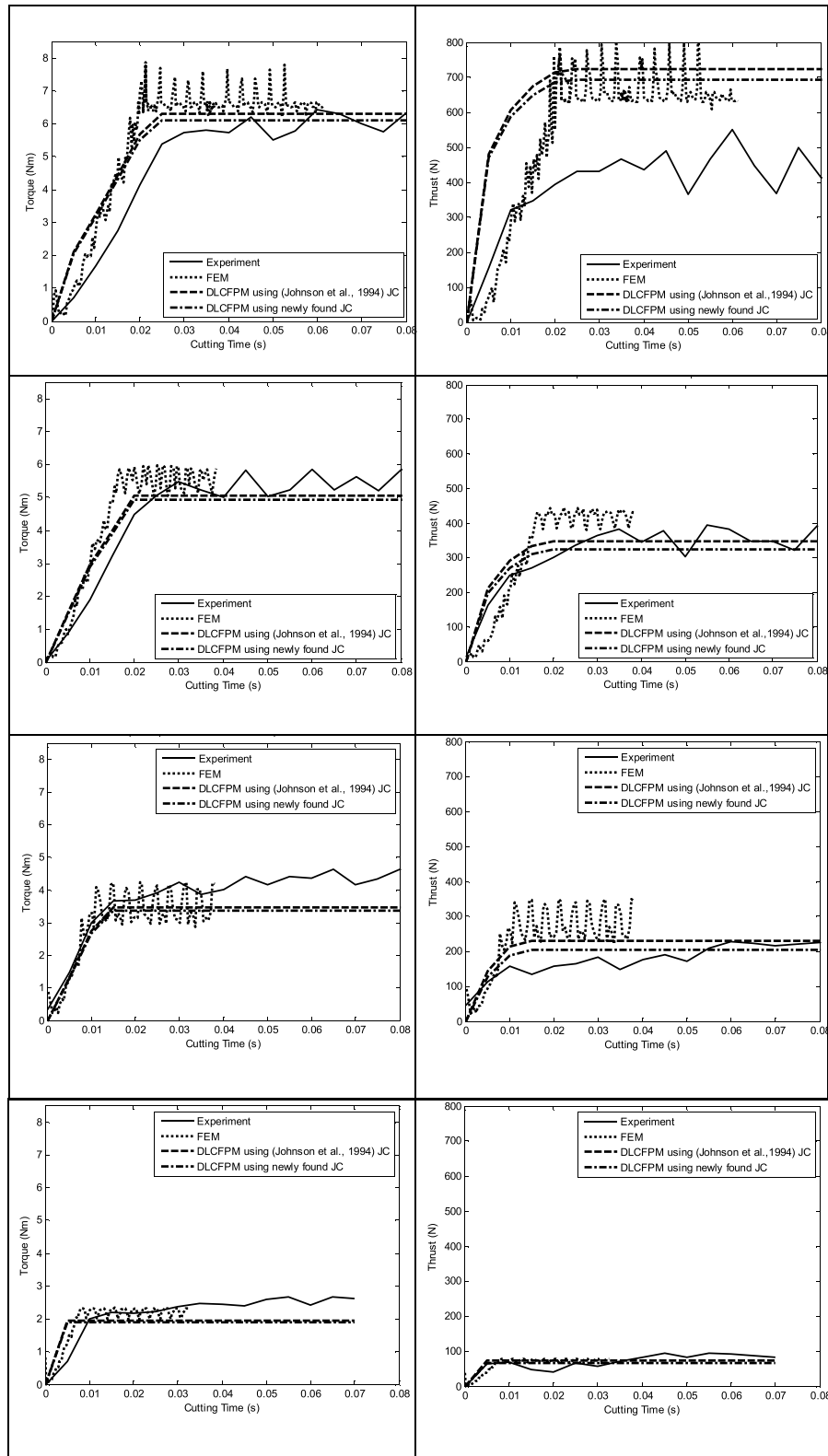


Fig. 13. Comparative plots of (L) torque and (R) thrust force profiles generated by DLCFPM and compared to experiments and FEM (spindle speed 9868 rpm, tool feed =0.64 mm/rev). From top to bottom pre-cored holes =2.5 mm 3.5 mm, 5.5 mm, and 7.5 mm, respectively.

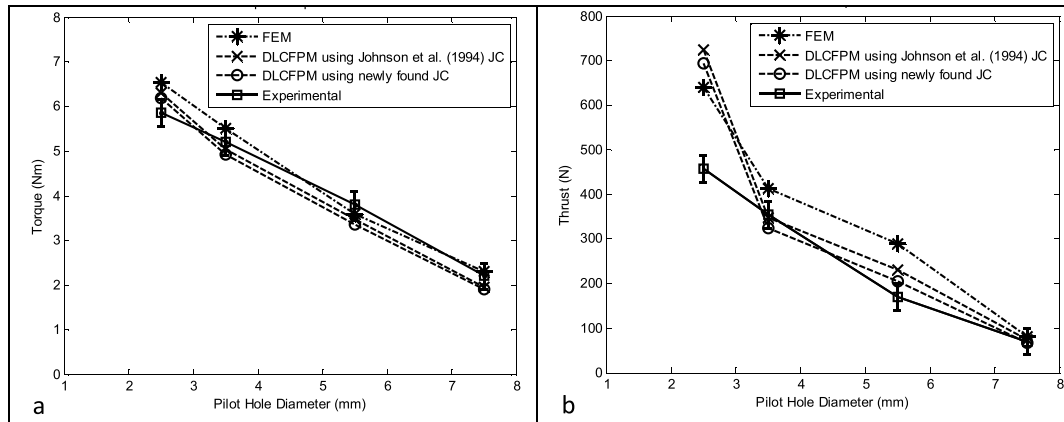


Fig. 14. (a) Torque and (b) thrust force results for experimental, FEM, and DLCFPM numerical results.

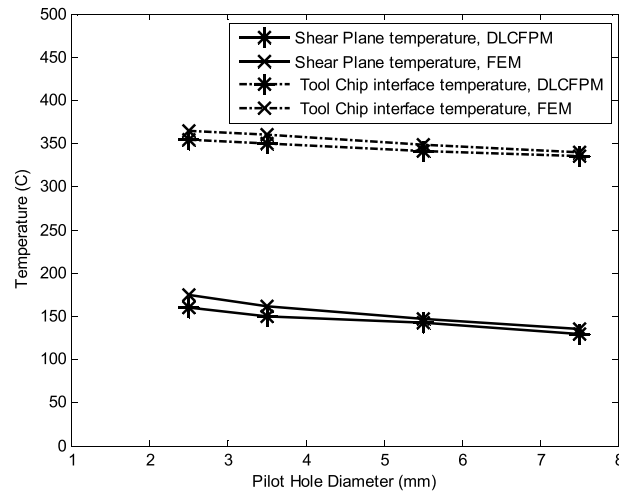


Fig. 15. Shear plane and tool-chip interface temperatures: DLCFPM versus FEM results.

Changing the convergence parameters induced only minor changes in determined parameter values. As compared to the control case, other runs converged to the same set of parameters but took longer to converge.

Validation of methodology using FEM simulations

The newly found JC parameters were employed in finite element modeling (FEM) simulations using DEFORM[®] software to predict the cutting forces in workpieces with pre-cored holes of 2.5 mm, 3.5 mm, 5.5 mm, and 7.5 mm. The numerically predicted forces were compared to those measured from the drilling experiments (Table 3).

FEM model

The drill point (Table 2) and pre-cored cylindrical workpieces were digitally replicated using 3D CAD and fed into the geometric preprocessor of DEFORM[®]. Workpiece geometry with 3.5 mm pre-cored pilot hole shown in Fig. 11(a). Tetrahedral elements used for mesh generation with an aspect ratio of 7 and maximum size equal to 30% of the feed. The workpiece was meshed using 17,354 elements with a minimum element size of 0.00014 mm. The tool

meshed with 14,354 elements of minimum element size of 0.005 mm. DEFORM[®] uses adaptive re-meshing that continuously update the mesh as the material deforms. Boldyrev et al. [23] demonstrated the applicability of JC type material model for cutting processes in FEM numerical modeling. The JC Al6061-T6 material parameters employed are those listed in Table 4. Contact conditions between the drill tool and workpiece control the friction and heat transfer at the interface between the two bodies. Adopted a sticking-friction criterion of 0.55 as reported by Gardner and Dornfeld [24] and aligned with DEFORM[®] developer manuals for drilling application. Considering that no coolant utilized, a suitable heat transfer parameter of 30 W/m²K was employed. To ensure stable simulation, a time step of 10⁻⁶s was utilized. Material separation is controlled by DEORM[®] mesh element splitting which occurs when the element reaches a critical plastic strain value.

FEM results

Matching with experiments, drilling simulations were conducted to a drilling depth of 4 mm guaranteeing full lip engagement. Fig. 11(b) shows a typical generated chip in the drilling simulation run for 3.5 mm pre-cored workpiece. Figs. 12

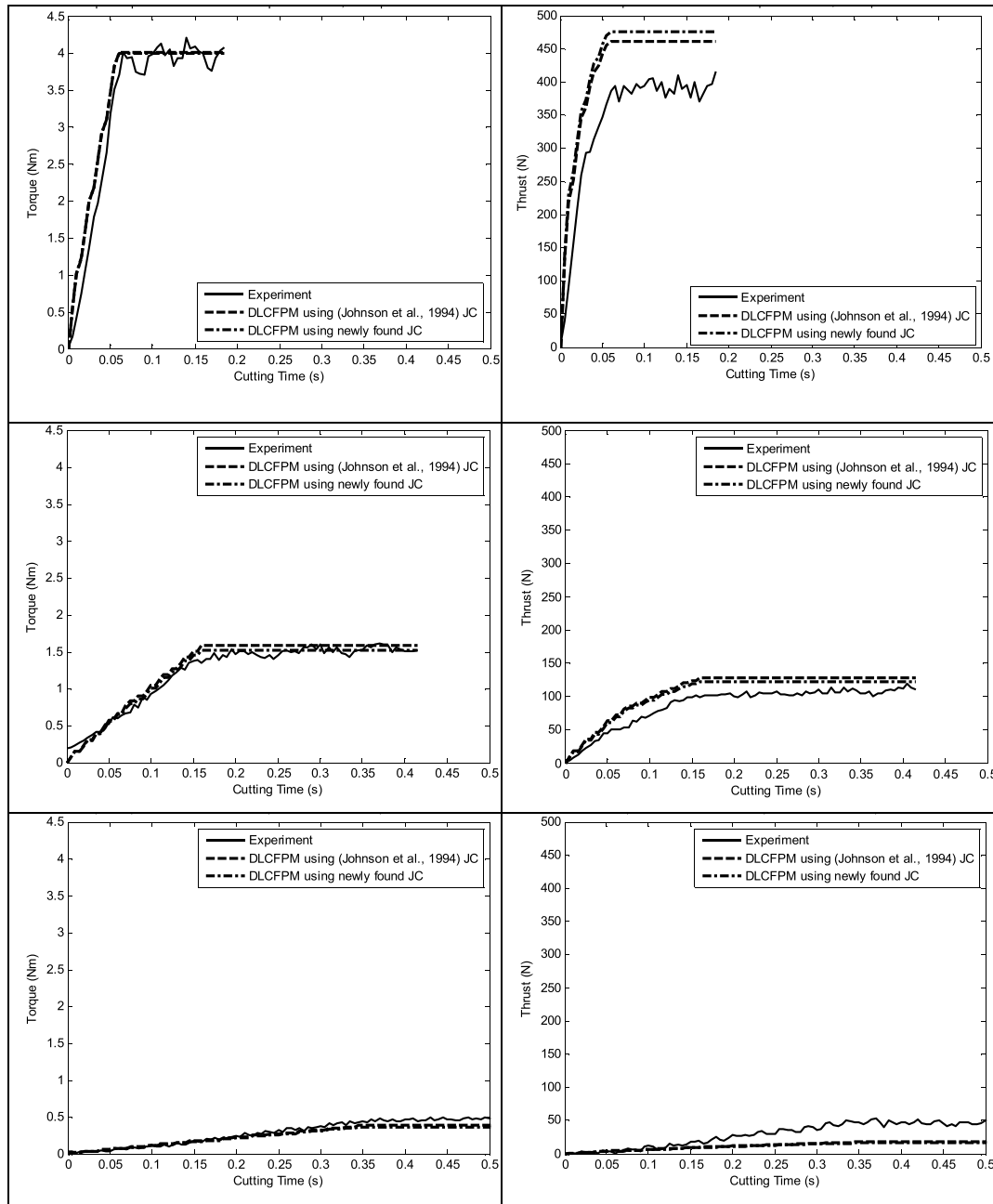


Fig. 16. Comparative plots of (L) torque and (R) thrust force profiles generated by DLCFPM and compared to experiments and FEM. Drilling parameters of pre-cored hole diameter, spindle speed, and tool feed rate are: (top) 3.5 mm, 6366 rpm, 0.32 mm/rev, (middle) 5.5 mm, 3183 rpm, 0.16 mm/rev, and (bottom) 7.5 mm, 1592 rpm, 0.08 mm/rev.

(a–d) are FEM generated plots of temperature, effective stress, strain, and strain rate, respectively, for 2.5 mm pre-core at 9868 rpm and 0.64 mm/rev. The maximum values of temperature and effective stresses are about 434 °C and 476 MPa, respectively, occurring at the tool-chip interface (FEM-generated torque and thrust profiles are reported in Fig. 13).

Comparison of predicted drilling forces versus FEM and experimental measurements

Fig. 13 are plots of torque and thrust force evolution profiles (spindle speed 9868 rpm, tool feed = 0.64 mm/rev) generated by

DLCFPM for (from top to bottom) 2.5 mm, 3.5 mm, 5.5 mm, and 7.5 mm pre-cored holes.

These numerical results are compared versus the results of FEM simulations and experiments for the same drilling parameters. DLCFPM-predicted profiles are calculated two ways: once employing JC flow stress parameters for Aluminum 6061-T6 as reported by Johnson et al. [5] and another using the JC parameters found in this work (317.54, 108.90, 0.0015, 0.43, and 1.29 for A, B, C, n, and m, respectively). These profiles show good agreement with each other, with the FEM simulations, and with the experiments.

Plotted in Fig. 14(a) and (b) are torque and thrust force values, respectively, recorded at full lip engagement versus pilot hole

diameter in pre-cored holes of 2.5 mm, 3.5 mm, 5.5 mm, and 7.5 mm cases. The plotted data correspond to full lip engagement torque and thrust values from the drilling experiments, FEM simulations, and DLCFPM results for reference JC parameters [5] and for JC parameters found in this work (9868 rpm and 0.64 mm/rev). For the experimental torque and thrust values, shown are error bars with respect to the arithmetic mean of conducted repeated experimental tests using t-student distribution at a 95% confidence interval. Fig. 14 shows good agreement between the incremental lip torque and thrust forces for DLCFPM results, FEM simulations, and experimental. Observed is a deviation from the experimental thrust force value for pilot-hole of 2.5 mm. The difference is attributed to the combined effect of high negative rake angle and slow cutting speed involved which may have caused deviation from the thick shear zone approach utilized to generate DLCFPM cutting forces.

For the same cutting parameters used to produce Figs. 13 and 14, co-plotted in Fig. 15 are an average shear plane (T_{AB}) and tool-chip interface temperature (T_{int}) found by FEM simulations and DLCFPM using the newly identified Al 6061-T6 JC parameters for pilot hole diameters of 2.5 mm, 3.5 mm, 5.5 mm, and 7.5 mm. Generated temperature values correspond to full lip engagement with the workpiece. The FEM values are determined by averaging found temperatures for nodes constituting the relevant primary and secondary deformation zones. While drilling pilot holes of diameter 2.5 mm and 7.5 mm, shear plane temperatures decreased from 176 °C to 133 °C while average tool-chip interface temperatures decreased from 365 °C to 328 °C. As cutting action approaches the drill margins, the effective rake angle of the engaged lip becomes more positive (Fig. 8) leading to more effective cutting.

Additional comparisons of DLCFPM-generated torque and thrust force profiles are made in Fig. 16. As a testament to the validity of the methodology, these generated profiles correspond to drilling parameters intentionally chosen to be different from those used to estimate the JC parameters (Section “Validation of methodology using FEM simulations”).

Fig. 16 plots the generated profiles for drilling of workpieces with (top) pre-cored hole of 3.5 mm, spindle speed 6366 rpm, and feed rate of 0.32 mm/rev (middle) pre-cored hole of 5.5 mm, spindle speed 3183 rpm, and feed rate of 0.16 mm/rev, and (bottom) pilot holes of 7.5 mm, spindle speed 1592 rpm, and feed rate of 0.08 mm/rev. DLCFPM-generated torque and thrust profiles with JC parameters found in this work compare favorably to those generated when utilizing DLCFPM with JC parameters reported by Johnson et al. [5] for 3.5 mm, 5.5 mm, and 7.5 mm pre-cored workpieces, also DLCFPM profiles track well with those experimentally measured.

Summary and conclusions

Based on Oxley’s extended thick shear zone formulation, developed in this work is a methodology dubbed the Drill Lip Cutting Prediction Methodology (DLCFPM). The methodology implemented utilizing a custom-written Matlab code, is applied to extract optimized Johnson–Cook (JC) flow stress parameters from a small number of drilling experiments. Experimental torque and thrust force profiles are generated from drilling tests using a 10 mm diameter drill on AL6061-T6 workpieces containing pre-cored pilot holes with diameters of 2.5 mm, 3.5 mm, 5.5 mm, and 7.5 mm so that the chisel edge is not engaged during the cut. The drilling experiments cover a wide range of drilling conditions with spindle speeds ranging from 1592 rpm to 9868 rpm and feed rates ranging from 0.08 mm/rev to 0.64 mm/rev. The DLCFPM solves for the JC

parameters so that as the drill’s lip engages with the pre-cored work, the JC parameters are automatically adjusted to minimize the difference between calculated and experimentally measured torque values. The methodology applied incrementally for each segment of the lip to which it is numerically subdivided. Curve fitting is performed based on a nonlinear least-squares optimization tool with a convergence criterion of 10^{-9} and maximum iteration number of 1000. Using initial randomly guessed values, all considered cases converged to the same set of JC parameter A, B, C, n, m of 317.54 MPa, 108.90 MPa, 0.0015, 0.43, and 1.29, respectively, as compared with Johnson et al. [5] reported values of 324 MPa, 114 MPa, 0.002, 0.42, and 1.34, respectively. The methodology robustness demonstrated by comparing torque and thrust evolution profiles using DLCFPM-found JC parameters versus experimental torque and thrust profiles. DLCFPM was shown to predict accurately the drilling torque forces but to a lesser extent the drilling thrust forces where some deviations from the experimental thrust values are observed. Future development of DLCFPM is planned to include the chip flow effect on thrust forces in the hope of improving the predictive accuracy of thrust forces.

Acknowledgments

Financial aid of the University Research Board (URB) at the American University of Beirut is acknowledged. The authors also wish to thank the Mechanical and Mechatronics Engineering Department at the University of Waterloo in Waterloo, Canada for facilitating the experimental data collection.

Appendix A. Supplementary data

Supplementary material related to this article can be found, in the online version, at doi:<https://doi.org/10.1016/j.cirpj.2019.06.001>.

References

- [1] Oxley, P.L.B., 1989, *The Mechanics of Machining: An Analytical Approach to Assessing Machinability*. Ellis Horwood Limited, Chichester, UK.
- [2] Shrot, A., Bäker, M., 2012, Determination of Johnson–Cook parameters from machining simulations. *Computational Materials Science*, 52/1: 298–304.
- [3] Hamade, R.F., Ismail, F., 2005, A Case for Aggressive Drilling of Aluminum. *Journal of Materials Processing Technology*, 166/1: 86–97.
- [4] Johnson, G.R., Cook, W.H., 1983, A Constitutive Model and Data for Metals Subjected to Large Strains, High Strain Rates, and High Temperatures. *Proceedings of the 7th International Symposium on Ballistics*.
- [5] Johnson, G.R., Peterson, E.H., Schonhardt, J.A., Stryk, R.A., Holmquist, T.J., Burns, C.R., 1994, User Instructions for the Final Version of the EPIC Research Code. Alliant Techsystems Inc., Brooklyn Park Mn.
- [6] Rule, W.K., 1997, A Numerical Scheme for Extracting Strength Model Parameters from Taylor Test Data. *International Journal of Impact Engineering*, 19/9–10: 797–810.
- [7] Dabboussi, W., Nemes, J.A., 2005, Modeling of Ductile Fracture Using the Dynamic Punch Test. *International Journal of Mechanical Sciences*, 47/8: 1282–1299.
- [8] Manes, A., Peroni, L., Scapin, M., Giglio, M., 2011, Analysis of Strain Rate Behavior of an Al 6061 T6 Alloy. *Procedia Engineering*, 10: 3477–3482.
- [9] Guo, Y.B., 2003, An Integral Method to Determine the Mechanical Behavior of Materials in Metal Cutting. *Journal of Materials Processing Technology*, 142/1: 72–81.
- [10] Naik, P., Naik, A., 2015, Determination of Flow Stress Constants by Oxley’s Theory. *International Journal of Latest Technology in Engineering Management & Applied Science IV*, 110–116.
- [11] Daoud, M., Jomaa, W., Chatelain, J.F., Bouzid, A., Songmene, V., 2014, Identification of Material Constitutive Law Constants Using Machining Tests: A Response Surface Methodology Based Approach. *WIT Transactions on the Built Environment*, 137:25–36.

- [12] Oxley, P.L.B., 1988, Modeling Machining Processes With a View to Their Optimization and to the Adaptive Control of Metal Cutting Machine Tools. *Robotics and Computer-integrated Manufacturing*, 4/1–2: 103–119.
- [13] Oxley, P.L.B., 1963, Rate of Strain Effect in Metal Cutting. *ASME Journal of Engineering for Industry*, 85/4: 335–337.
- [14] Lalwani, D.I., Mehta, N.K., Jain, P.K., 2009, Extension of Oxley's Predictive Machining Theory for Johnson and Cook Flow Stress Model. *Journal of Materials Processing Technology*, 209/12–13: 5305–5312.
- [15] Lin, G.C.I., 1978, Prediction of Cutting Forces and Chip Geometry in Oblique Machining From Flow Stress Properties and Cutting Conditions. *International Journal of Machine Tool Design and Research*, 18/3: 117–130.
- [16] Wiriyacosol, S., Armarego, E.J.A., 1979, Thrust and Torque Prediction in Drilling From a Cutting Mechanics Approach. *Annals-Manufacturing Technology*, 87–91.
- [17] Stabler, G.V., 1951, The Fundamental Geometry of Cutting Tools. *Proceedings of the Institution of Mechanical Engineers*, 165/1: 14–26.
- [18] Boothroyd, G., 1963, Temperatures in Orthogonal Metal Cutting. *Proceedings of the Institution of Mechanical Engineers*, 177/1: 789–810.
- [19] Oxley, P.L.B., 1982, Machinability: A Mechanics of Machining Approach. *On the Art of Cutting Metals–75 Years Later: A Tribute to FW Taylor*, vol. 7. A.S.M.E. PED. p. 37. 1982.
- [20] Williams, R.A., 1974, A Study of the Drilling Process. *Journal of the Institution of Engineers*, 96/4: 1207.
- [21] Shin, Y.C., Waters, A.J., 1997, A New Procedure to Determine Instantaneous Cutting Force Parameters for Machining Force Prediction. *International Journal of Machine Tools and Manufacture*, 37/9: 1337–1351.
- [22] Hamade, R.F., Seif, C.Y., Ismail, F., 2006, Extracting Cutting Force Parameters from Drilling Experiments. *International Journal of Machine Tools and Manufacture*, 46/3: 387–396.
- [23] Boldyrev, I.S., Shchurov, I.A., Nikonov, A.V., 2016, Numerical Simulation of the Aluminum 6061-T6 Cutting and the Effect of the Constitutive Material Model and Failure Criteria on Cutting Forces' Prediction. *Procedia Engineering*, 150:866–870.
- [24] Gardner, J., Dornfeld, D., 2006, Finite Element Modeling of Drilling Using DEFORM. Consortium on Deburring and Edge Finishing Laboratory for Manufacturing and Sustainability UC Berkeley, .